Electrical Power and Energy Systems 162 (2024) 110217

Contents lists available at ScienceDirect

International Journal of Electrical Power and Energy Systems

journal homepage: www.elsevier.com/locate/ijepes

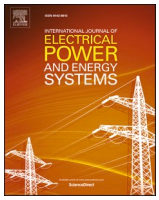

Harmonic measurement and analysis system for characterization of adjustable speed drives

Angel Arranz-Gimon [a], Angel Zorita-Lamadrid [b], Daniel Morinigo-Sotelo [b], Vanesa Fernandez-Cavero [c], Oscar Duque-Perez [b,*]

[a] Department of Electronic Technology, Universidad de Valladolid, 47011, Valladolid, Spain
[b] Department of Electrical Engineering, Research Group ADIRE, ITAP, Universidad de Valladolid, 47011, Valladolid, Spain
[c] Department of Electromechanical Engineering, Electrical Engineering Area, Universidad de Burgos, 09001, Burgos, Spain

ARTICLE INFO

Keywords:
Adjustable Speed Drive (ASD)
Electric power quality
Harmonic distortion
Standard IEC61000-4-7
Time aggregation
Frequency grouping
Induction motor

ABSTRACT

Variable speed drives, commonly employed for motor speed control, incorporate electronic converters that emit harmonics to both the power grid and the motor-load system. These harmonics can have adverse effects on the motors, necessitating the experimental measurement of their diverse and unpredictable harmonic content. To perform these measurements on the input side of the drives or power grid, commercial quality analyzers are available, but they are not prepared to perform these measurements on the motor-load or output side of the drive. The outputs of the drives generate a significant harmonic and interharmonic content across a wide range of low and high frequencies, coupled with variable fundamental frequencies. Consequently, the development of a specialized measurement system tailored to these signal characteristics becomes imperative. This paper presents a harmonic measurement and analysis system specifically designed for frequency inverter's output signals, which adheres to international standards that standardize measurements and includes new features to evaluate converter signals not available in commercial meters. By utilizing this system, frequency groupings and distortion rates are obtained to comprehensively analyze the power quality of commercial drives under realistic operating conditions, thus enabling the early detection of potential failures and the implementation of preventive measures.

1. Introduction

Adjustable Speed Drives (ASD) play an important role in the industry, being applied mainly in the speed control of induction motors. ASDs consist of power electronic converters that behave as non-linear loads that generate harmonics, affecting not only the power grid, but also the load. These harmonics cause adverse effects on the induction motors fed by ASDs, such as overheating, insulation problems, noise and torque oscillations, reducing their useful life. It is therefore advisable to measure this harmonic content in order to characterize the quality of the energy supplied by this equipment and thus prevent possible failures in the connected equipment.

The frequency response of commercial inverters is dependent on the specific switching and fundamental frequencies employed at any given time, the different modulation and control strategies [1–3], the state of the supply network and the load-motor. This frequency response becomes even more unpredictable when the drives are connected to faulty motors, which cause additional harmonic content [4–6]. Moreover, manufacturers do not usually provide detailed information on the internal constitution and harmonic emission of ASDs and, when they do, this information is provided only for the optimum situation in terms of emission when the equipment is operating at nominal load conditions. Thus, it is necessary to experimentally determine the harmonics produced by ASDs under real operating conditions.

Several authors have quantified the harmonic pollution on the grid side when connecting power converter equipment producing high harmonic content at high and low frequencies, such as solar and wind renewable energy generation systems [7,8], loads such as low consumption lighting systems and electric vehicle chargers [9,10], or even variable frequency drives [11–13]. Besides, commercial power quality analyzers are available that quantify the harmonic emission according to international harmonic measurement standards. Such analyzers, as well as those proposed in the literature, have the advantage of being optimized to measure on the grid side, but the disadvantages of not being prepared to synchronize their measurements with variable fundamental

* Corresponding author.
E-mail address: oscar.duque@uva.es (O. Duque-Perez).

https://doi.org/10.1016/j.ijepes.2024.110217
Received 30 November 2023; Received in revised form 17 May 2024; Accepted 1 September 2024
Available online 13 September 2024

Nomenclature

Abbreviations

ASD	Adjustable Speed Drive
DFT	Discrete Fourier Transform
gH	Harmonic group
gH_aggreg	Harmonic group aggregated in time
gIH	Interharmonic group
HW	Hanning Window
IEC	International Electrotechnical Commission
RW	Rectangular Window
SgH	Harmonic subgroup
SgIH	Interharmonic subgroup
$TH\&IHDg_{HF}$	Total Harmonic and Interharmonic rate of High Frequency (from 40th harmonic up to 20 kHz)
$TH\&IHDg_{LF}$	Total Harmonic and Interharmonic rate of Low Frequency (up to and including harmonic 40, according to the current value of the fundamental *Fn*)
$TH\&IHDg_{LF\&HF}$	Total Harmonic and Interharmonic rate of total Low and High frequency
THD	Total Harmonic Distortion (up to and including harmonic 40, according to the current value of the fundamental *Fn*)
THD_aggreg	Total Harmonic Distortion aggregated in time

Parameters

Df_t	Theoretical or standard-indicated frequency resolution of 5 Hz (inverse of tw_t)
D_HF	Size of each high frequency group
Fs	Sampling frequency
Fsup	Upper frequency of the harmonic or low frequency zone
Fsup2	Upper frequency of the high frequency zone
tw_t	Theoretical or standard-indicated analysis window of 0.2 s

Variables

bar_sp	Spectral bar obtained after performing DFT
Df	Frequency resolution in general, without specifying whether it is theoretical or real
Df_r	Frequency resolution, inverse of tw_r, really used for the current fundamental frequency *Fn*
Fn	Fundamental frequency of the analyzed signal
h	Number of harmonic
H	Pure harmonic
I_L	Line Current
J	Total number of consecutive *tw* windows to be aggregated in the *Tw* total time
JJ	Actual number of *tw* window to be aggregated in the *Tw* total time
k	Number of spectral bar
N	Integer number of periods of *Fn* contained in the short *tw* windows. *N* is the same as the number of spectral bars between harmonics or multiples of *Fn*
n	Number of sample
Signal_Ref	Reference signal to synchronize analysis windows with fundamental frequency *Fn*
tot_bars	Total number of spectral bars analyzed
tw	Analysis window in general, without specifying whether it is theoretical or real
tw_r	Analysis window really used taking into account the current fundamental frequency *Fn*
Tw	Total analysis time or total aggregation time (divided into *tw* short windows)
Vector_crosses	Vector of zero crossings. Indicates the positions at which the reference signal changes sign
V_{FN}	Phase Voltage
Vref	Filtered phase voltage used as synchronism reference

frequencies such as those of the ASD signals, nor to reach a wider frequency range than in the network signals (the converter load side presents abundant harmonic and interharmonic content in the harmonic frequency range, up to 2 kHz, and especially in the supra-harmonic frequency range, 2–150 kHz [14–16]), nor to adapt their measurement parameters to the stationarity of the inverter signals, and they do not incorporate new distortion rates that allow differentiating harmonic and interharmonic components and distinguishing between low and high frequency measurements, as is needed to evaluate the quality of the ASD output signals.

The International Electrotechnical Commission (IEC) defines, in its power quality measurement standards 61000-4-7 and 61000-4-30 [17,18], the methods for the measurement of harmonics and interharmonics in the electrical network. In IEC standards, the discrete Fourier transform (DFT) is the basic analysis tool to obtain the rms values of harmonic and interharmonic groupings. Several authors have described measurement methods based on the DFT and IEC standards [19–24], and for supraharmonic frequencies [25–28]. Comparing the different harmonic analysis methods, parametric, nonparametric and hybrid [29–32], DFT remains the simplest technique with low computational burden, flexible and robust, and with a good compromise between accuracy and simplification [33]. Given the variety of existing ASD spectra on the market, with diverse and unpredictable harmonic contents, DFT-based techniques are the most suitable since they do not require prior knowledge of the position and number of harmonic components of the considered signals, thus allowing to analyze the harmonic behavior of any commercial drive. To perform DFT, the standard 61000-4-7 indicates the use of rectangular windows (RW) of a constant length of 12/10 cycles for 60/50 Hz electrical networks, which is equivalent to about 0.2 s and a resolution of 5 Hz. The main drawback of DFT is spectral leakage, which produces misleading measurements of the harmonic content of the analyzed signal. Spectral leakage is caused by interharmonic frequencies and, in general, by frequencies that are not synchronized with the standard frequency resolution of about 5 Hz, if the analysis window length indicated in the standards is used. It is therefore very important that the analysis window contains an integer number of periods of the fundamental frequency, regardless of whether the resulting window is exactly 0.2 s, to avoid significant spectral leakage. caused by desynchronization of the window with the higher amplitude component which is the fundamental.

Taking into consideration the aforementioned factors and a thorough examination of the relevant literature, it becomes evident that there is currently no existing system that effectively addresses the challenge of measuring signals like the output signals of ASDs, which exhibit variable fundamental frequencies and diverse harmonic contents. To fill this gap, this paper introduces a novel harmonic measurement and analysis procedure specifically designed to experimentally characterize ASDs. This system extends the capabilities of commercial power quality analyzers, oriented to analyze network signals, and improves their performance by introducing a new methodology to analyze inverter output signals with variable and dispersed harmonic content. The results of the developed measurement system are presented in the form of frequency groupings and distortion rates, which allow characterizing the power of the tested drives. In order to experimentally verify the developed system, several tests have been carried out, analyzing the measurements obtained with the described system.

The rest of this paper is organized as follows: Section 2 presents the problem of measuring the output signals of ASDs and the requirements of the measuring system. Then, in section 3, the measurement system proposed is explained, describing both hardware and software, as well as

the way used to solve the problems related to spectral leakage by means of an adequate synchronization of the measurements to reduce the generation of leakage, and the groupings both in frequency and in time to mitigate its effects. In section 4, experimental results are presented and analyzed, testing induction motors fed by variable frequency drives with different harmonic contents. Finally, Section 5 presents the conclusions derived from this study.

2. Requirements for measuring drive signals: Key characteristics

Based on the IEC standard, the measurement method for characterizing drives according to their harmonic content must incorporate additional features that complement the performance of commercial power quality measuring equipment, intended only for network signals. It must be possible to flexibly configure the values of various parameters, which in commercial meters are usually fixed. Specifically, the designed system should have the following features:

- To allow measurements at different fundamental frequencies. It must be possible to measure drive output signals that are not always at nominal frequencies of 50 Hz or 60 Hz. To achieve this, the synchronism of the measurements must be readjusted to the fundamental harmonic present in each particular test, recalculating the number of cycles of the current fundamental necessary so that the analysis window is always as close as possible to that recommended in the standards, in order to unify the measurements and make them comparable with each other.
- Possibility to choose the resolution in time and frequency, varying the size of the sampling window for this purpose.
- To adapt the aggregation times to values appropriate to the specific nature of the signals present at the output of the drives.
- To modify the frequency groupings as they contain different numbers of spectral bars depending on the value of the current fundamental frequency.
- To measure a wider range of frequencies, above the 9000 Hz indicated in the IEC 61000-4-30 standard, (since the converters have higher switching frequencies than those usually measured in the power grid).
- To find harmonic distortion rates for different frequency ranges, capable of distinguishing and measuring harmonics and interharmonics, and capable of differentiating high-frequency content from low-frequency content, which improve and complement the rates defined in standards.

Since the purpose of the measurement system is harmonic analysis, the analyzed signals (stator currents and phase-neutral voltages) will be measured under stationary conditions only. The possible time variability of the signals provided by the frequency converters makes it necessary to obtain a compromise between spectral and time resolution when choosing the window or sampling time during which the measurements are taken (due to the uncertainty principle, it is impossible to improve both time and frequency resolutions at the same time [34–36]), hence, the IEC standard 61000-4-7 recommends utilizing 0.2 s windows for network signals, taking into account the degree of stationarity of these signals. But for analyzing drive output signals, this window length or time resolution can be conditioned to the characteristics of the signal under consideration [37]. The chosen time resolution influences the frequency resolution and thus the accuracy of the resulting measurements. In the system developed in this article, we will use windows of the closest duration to the 0.2 s indicated by the standards in order to unify all the measurements, taking into account that a variation of this value can be allowed, since for quasi-stationary harmonics in industrial signals the real analysis window tw_r can vary from 0.1 to 0.5 s according to their dynamic behavior [38].

To minimize spectral leakage, before applying the DFT measurements must be synchronized with the acquisition window. It is crucial to address this issue as the most significant leakage stems from frequency components with higher amplitudes. For this purpose, standard 61000-4-7 states that the *tw* analysis window must be synchronized with each integer number of cycles of the fundamental harmonic that add up to the nearest 0.2 s, with a maximum permissible error of $\pm$ 0.03 % over the duration of the sampling window. Specifically, the standard indicates 10/12 periods for 50/60 Hz networks respectively. In the case of inverters, in order to try to maintain a sampling window as close as possible to that indicated in the standard, with the purpose of unifying the measurements and making them comparable with those obtained with the standards, the synchronism of the measurements must be adjusted to the current value of the fundamental harmonic.

In case of loss of synchronism, the Hanning window (HW) can be used to reduce the leakage. Although the use of HW reduces the effects of leakage between distant tones, however, it worsens the resolution when measuring near tones [23]. For harmonic analysis using the groupings recommended in the IEC standard, Tarasiuk, Barros and R.I. Diego [39–41], showed that the use of the rectangular window was preferable to the Hanning window in any of the groupings defined by the standard. For the measurement of high frequencies (above the 40th harmonic) as well as interharmonics in general, the same standard states that it is no longer necessary to stay within the error margin for synchronism and the rectangular window can be used.

Other ways to reduce leakage are to improve the synchronization by adjusting the length of the DFT window. The idea is that each sampling window should contain an integer number of samples with up to 0.03 % error and for this the sampling frequency should be an integer multiple of the fundamental frequency of the analyzed signal, actually measured in real time [30]. One way can be by modifying the sampling rate online, (before performing this sampling), so that it matches or is a multiple of the actually measured fundamental frequency, thus acquiring a whole number of samples that synchronizes or fits into an also complete number of periods; or another way can be by interpolating values between samples, (modification, in this case via software and not online of the sampling rate, which is performed after data acquisition), to achieve identical result [42,43]. But the online modification of the sampling rate requires the possibility to modify this frequency and to detect the fundamental, using for example PLLs; while the interpolation algorithms modify the initial nature of the signal, besides not being accurate when harmonics and interharmonics coexist in the analyzed signal [37], as occurs in the output signals of variable speed drives.

In addition, to reduce the effects of spectral leakage after applying the DFT, and since the developed system is based on the IEC quality measurement standard for harmonics and interharmonics, two levels of measurement grouping will be performed:

- A first level of frequency groupings, in groups and subgroups, harmonics and interharmonics, with a spectral resolution of about 5 Hz (windows with the closest value to 0.2 s, considering the aforementioned margin of 0.1 to 0.5 s for harmonics measurement) [17,38]. At high frequencies, the standards recommend wider groupings (of 200 Hz), always respecting the 0.2 s – 5 Hz resolution, and thus covering the interharmonic groupings around multiples of the switching frequency, located in the high frequency region.
- A second level of grouping in time, taking successive measurements until completing 3 s (15 measurements of 0.2 s), which can be extended to other levels higher in duration [18].

Frequency grouping effectively captures most of the spectral leakage generated within each group, although with some dispersion of leakage beyond its boundaries. The grouping in time reduces the loss of information due to the leakage and reduces the error due to the lack of stationarity of the signal, increasing the accuracy and stability of the measurements and compressing the information [39]. The developed measurement system must also adapt the aggregation times, as well as the frequency groupings and distortion rates of the standard, to values

appropriate to the specific nature of the signals present at the output of the drives.

According to IEC standards, time aggregation can only be performed at intervals of 3 s, 10 min or 2 h, although these times are intended only for mains signals and must be adapted to the characteristics of the drive signals. These times are different according to the test conditions analyzed (motor and load, type of power supply and control) and even the type of measurement (single harmonic, harmonic groups, distortion rates, etc.), but a minimum value can be established that is valid for all tests. In [44] we verified that, for the case of low power variable frequency drive signals, an aggregation time of about 10 s is sufficient to improve the results, so this will be the time used in the system developed in this work.

The distortion rates defined in the standards, valid for measurements in the network, must be improved to adapt them to the characteristics of the output signals of the drives, and therefore must admit different fundamental frequencies and their multiples or corresponding harmonics, must also include the ability to measure interharmonics, both in low and in a wider range of high frequencies, and avoid in the normalization the appearance of continuous and interharmonic components in the denominator that can produce uncertain results. The distortion rates used in this proposal are based on the specific rates we described in [45] and include the aforementioned improvements of the rates defined in the standards in order to correctly measure distortion in ASD output signals.

3. Harmonic measurement and analysis system in frequency inverters

In this section, the developed system will be described, starting with the block diagram that illustrates the general hardware part of the system, followed by the algorithm or software and the synchronism method used by the developed measurement system.

3.1. General description of the hardware of the measurement system

The proposed measurement and analysis system samples and analyzes the electrical output signals of a frequency inverter that excites an induction motor. For this purpose, a personal desktop computer with an internal data acquisition card and an external adaptation or interface module between the tested equipment and the measurement system are used, as shown in Fig. 1.

The three phase voltages and the three output currents of the frequency converter are first electrically isolated and conditioned by means of an interface card based on Hall effect probes (LEM probes, models LA100P and LV25P, for measuring current and voltage, respectively), and then sampled and digitized by means of a National Instruments

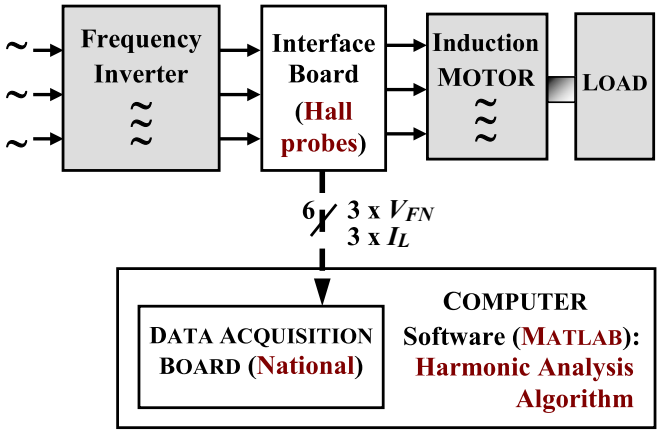

Fig. 1. Block diagram of the measurement and analysis system developed.

PCI6250 acquisition card, integrated into a personal computer. The harmonic content above 20 kHz has not been considered, since it is already somewhat attenuated due to the frequency response of the Hall voltage probes, nor has the continuous component been taken into account, since it accumulates the offset errors of the entire measurement system. The sampling frequency *Fs* has been chosen high enough (80 kS/s) to meet all the necessary specifications (to measure the high harmonics of the drives, to reduce the noise reflected from the high part of the spectrum due to aliasing, and to reduce the synchronism errors due to the sampling interval). The Matlab software package is used both for the control of the signal acquisition and for the subsequent processing and analysis of the resulting data by means of the software-algorithm described in the following subsection.

3.2. Harmonic analysis algorithm of the developed measurement system

The software part or algorithm used in the developed measurement system is explained below, starting with a general introduction, followed by a more detailed analysis of the algorithm in the next subsection 3.2.2. The synchronization of the analysis windows, taking into account the particularities of the analyzed signals, will be explained in greater depth in subsection 3.3.

3.2.1. General description of the developed algorithm

The schematic represented in Fig. 2 and the flow chart in Fig. 3 summarize the proposed analysis algorithm. The line current I_L and phase voltage V_{FN} signals sampled at the output of the inverter are analyzed during the total analysis time *Tw*. If the harmonic analysis of the signal based on the IEC standard is performed, it is necessary to first divide the total analysis time *Tw* into *J* consecutive short *tw* windows with the duration closest to 0.2 s containing an integer number *N* of periods of the actually measured fundamental frequency *Fn* of the analyzed signal. In this way, the short *tw* analysis windows will be synchronized with the fundamental frequency *Fn* and thus reduce spectral leakage production. In addition, it is also necessary to know the fundamental frequency *Fn* to be able to perform the frequency groupings, indicated in the same standard, since the number of spectral bars that integrate the different harmonic groupings depends on the current value of *Fn*. It should be remembered that the fundamental frequency *Fn* is variable, in order to control the speed of the excited motor, so that, in principle, its value is unknown. Therefore, to find the value of *Fn*, a first DFT is performed using a window with a high sampling time (10 s), and consequently a high frequency resolution ($Df = 0.1$ Hz), and poor time resolution (due to the uncertainty principle), in which it is not important to be accurate in the amplitude, but it is important to be accurate in the value of the frequency *Fn*.

If the zero-crossing detection method is used to divide the total analysis time *Tw* into short windows, the number of zero crossings of the synchronism signal during each short window ($2 \cdot Fn \cdot tw$) is variable and depends on the output frequency (*Fn*) of the drive, which is why *Fn* is found after this first DFT. To synchronize the short analysis windows, the phase voltage signal V_{FN}, duly filtered, is used as the synchronism reference, as shown in the upper part of Fig. 2.

Once the total analysis time *Tw* is divided into short windows tw_r, well synchronized with the fundamental *Fn*, new and successive DFTs are applied on these *J* consecutive short windows, this time with worse frequency resolution ($Df_r \approx 5$ Hz) but better resolution in time ($tw_r \approx 0.2$ s), thus fulfilling the compromise between both resolutions specified in the regulations for the type of signals analyzed. With the spectral bars obtained in each DFT, separated by about 5 Hz, the basic frequency groupings (such as groups and subgroups, harmonic and interharmonic) are performed and by adding again the previous ones, more complex groupings such as distortion rates are calculated.

Finally, the results obtained in the *J* windows analyzed are aggregated over time, considering the total analysis or aggregation time *Tw*, as shown in the lower part of the diagram in Fig. 2 and the flowchart in

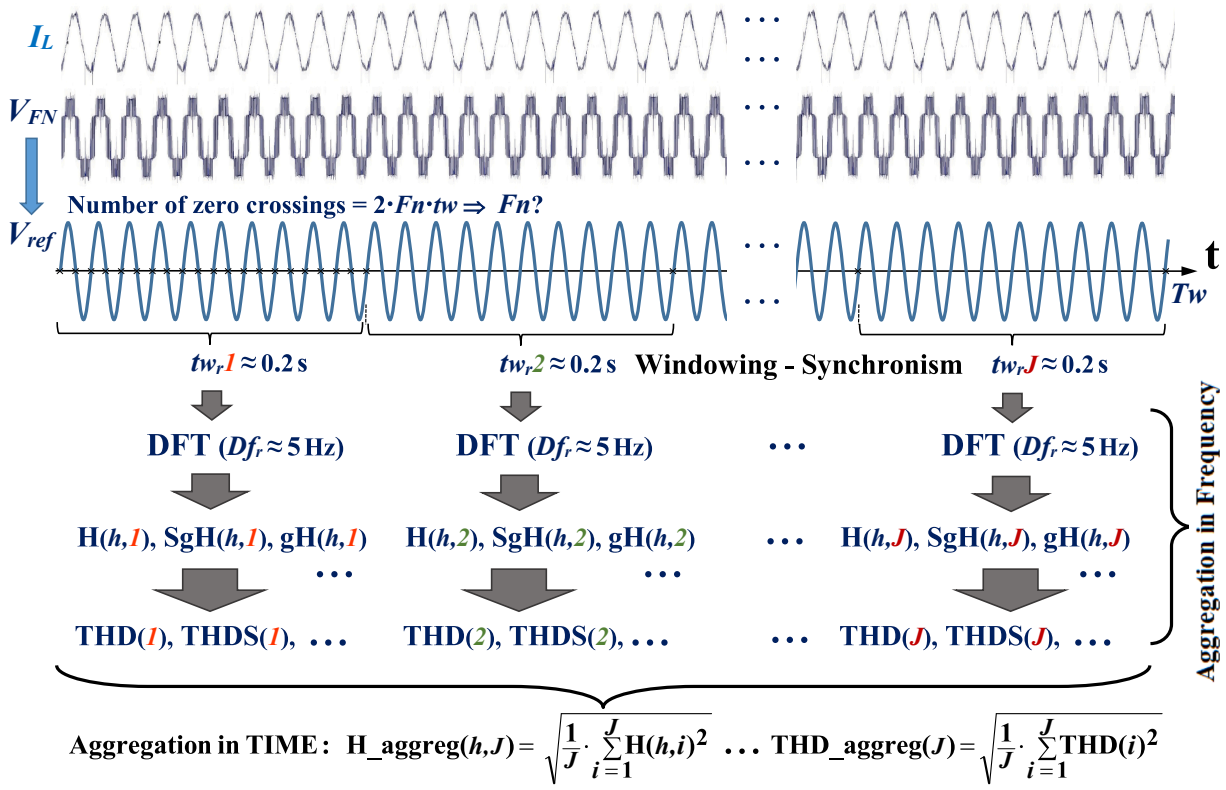

Fig. 2. Summary of the process of measuring harmonic distortion in inverter signals, based on IEC standards, considering the two levels of grouping, in frequency and in time.

Fig. 3.

The schematic in Fig. 2 and the flowchart in Fig. 3 have summarized in a general way the complete process, from the acquisition of the output signals from the converter to the final obtaining of the frequency groupings and time-aggregated distortion indices, and in the following subsection each of these steps will be further detailed, leaving for section 3.3 the explanation and verification of the synchronism method used for clarity.

3.2.2. *Detailed description of the developed algorithm*

The flow chart in Fig. 4 describes in more detail the stages into which the standards-based analysis algorithm used by the system developed for harmonic characterization of drives is divided.

First, initializations are performed for several parameters such as the sampling frequency *Fs* (80 kHz), the upper frequency of the harmonic or low frequency zone *Fsup* (default of 40 times the value of *Fn*), the upper frequency *Fsup2* of the high frequency zone (default 20 kHz), the size of each high frequency group *D_HF* (of 200 Hz), the approximate size of the standard acquisition window tw_t (0.2 s) and its inverse or standard frequency resolution Df_t (5 Hz), and the total analysis time *Tw* (10 s) which coincides with that used for time aggregation. From here, other parameters derived from the previous ones are obtained, such as the total number of consecutive *tw* windows to be aggregated in time, *J*, and the total number of spectral bars, *tot_bars*, contained within the analyzed frequency range and separated by the basic resolution *Df*.

Next, the information of the sampled signals of line current I_L and phase voltage V_{FN} is loaded. The fundamental frequency of these signals, *Fn*, is detected by a first application of the DFT, simply looking for the frequency corresponding to the spectral bar with the highest amplitude. With this value of *Fn*, the integer number of periods *N* of *Fn* can already be calculated to obtain the tw_r window closest to the standard value of 0.2 s and thus divide the total sampling time *Tw* into short windows. Moreover, this number of periods *N* is the same as the number of spectral bars between harmonics or multiples of *Fn*.

The next step is the division of the total aggregation time *Tw* in consecutive windows of size tw_r (with a value close to 0.2 s) and synchronous with the period of the fundamental harmonic *Fn*, in order to be able to apply DFT transforms on each of them, thus respecting the compromise between time and frequency resolution sought for this type of pseudo-stationary signals. In order to divide the total time *Tw* into short *tw* windows, the positions of the samples of the original analyzed signal where the periods of its fundamental frequency *Fn* begin are stored in a vector of zero crossings (as occurs every two zero crossings in a sinusoidal signal). This vector will then be used to address the signal samples at the start and end times of each successive tw_r basic window.

Once the total aggregation time *Tw* has been divided into *J* short windows tw_r, successive DFTs of low frequency resolution, but high time resolution, are applied on them. Each of these DFTs is applied on the successive short windows separated "2·*N*" zero crossings, since *N* is the number of periods of *Fn* contained in each short window tw_r, and in each period there are 2 zero crossings. If with the first DFT *Fn* was found, now these second DFTs are the ones that actually produce the spectral bars separated by about 5 Hz with which all the frequency groupings and distortion rates will be calculated later.

The calculation of the harmonic or low-frequency frequency groupings, not yet aggregated in time, (pure harmonic H, harmonic subgroup SgH, harmonic group gH, interharmonic subgroup SgIH and interharmonic group gIH) is described in the flow chart depicted in Fig. 5. The values of the groups and subgroups are calculated from those related to the first harmonic (counter $h = 1$ and number of spectral bars equal to $h{\cdot}N$), until the total number of spectral bars is reached. The value of the spectral bar number *k* at the beginning of each group is increased in each iteration by "$k + N$" 5 Hz spectral bars, since *N* represents the total number of them contained between harmonic and harmonic. Depending on whether *N* is even or odd, the way to find the value of a harmonic group changes slightly. For even *N*, (case of frequencies such as mains,

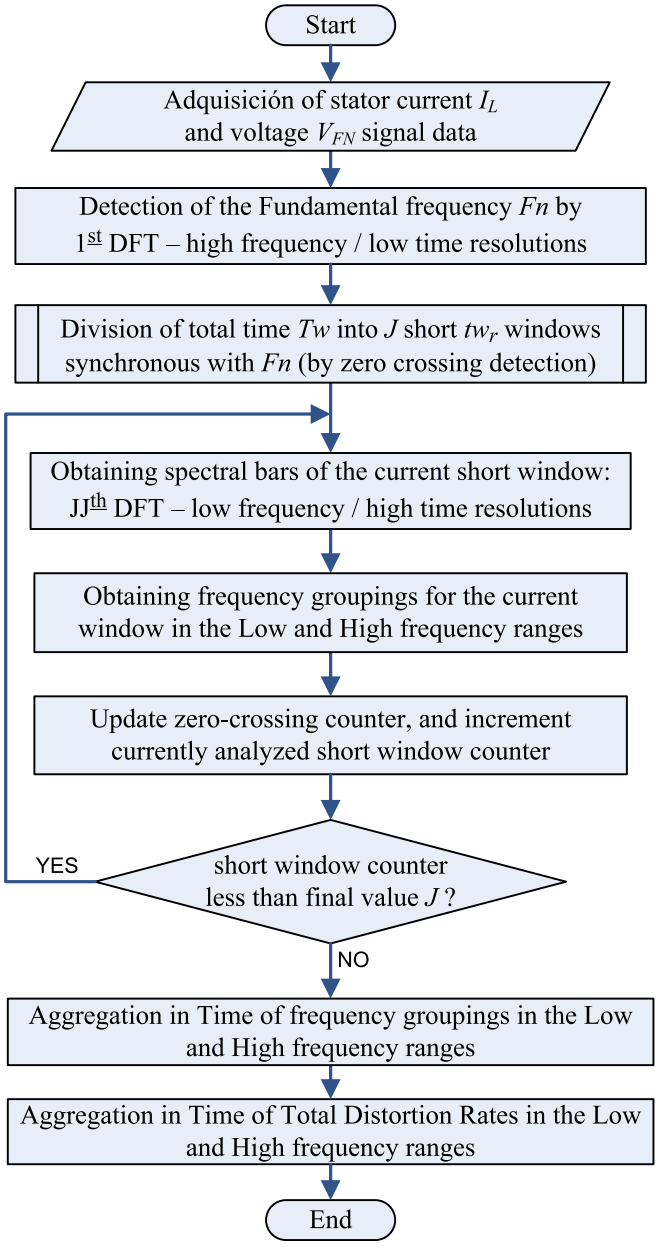

Fig. 3. Summary flowchart of the harmonic analysis algorithm.

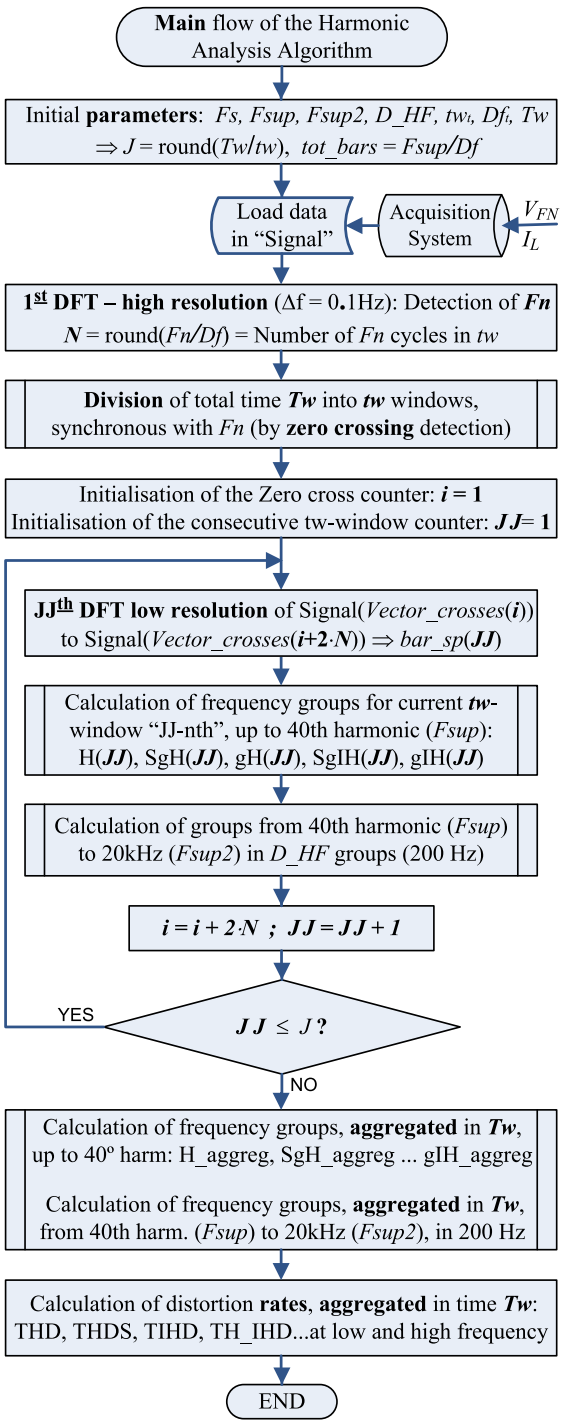

Fig. 4. Main flowchart of the algorithm of harmonic analysis.

50 or 60 Hz), there is an odd number of bars between harmonic and harmonic, so contiguous harmonic groups share the energy of the interharmonic bars "$(h{\cdot}N) \pm (N/2)$" that are in between them.

The high frequency groups are calculated in groups of 200 Hz, as recommended in the annex of standard 61000-4-7 [17], and always using the spectral bars separated by 5 Hz calculated previously. The lower frequency *Fsup* is selected in each test according to the value of the fundamental harmonic *Fn*, and it is chosen as 40·*Fn*.

In all the above frequency groupings, matrices of values are created whose indices are, on the one hand, the harmonic number *h*, covering the frequency range considered in each case; and on the other hand, the number *JJ* of short *tw* window considered in the current analysis, within the total *Tw* aggregation time considered. For example, the content of gH(3,50) corresponds to the third harmonic group analyzed in the 50th short window *tw*.

On the other hand, with groupings already aggregated in time, as for example gH_aggreg(3,50), the value of the third harmonic group is also obtained, but now aggregating the values of the first 50 consecutive windows. The aggregations over time are calculated by the square root of the arithmetic mean of the squares of the input values [18]. For example, the harmonic group of order *h* aggregated over time for the first *JJ* windows is obtained with the following expression:

$$gH\_aggreg(h, JJ) = \sqrt{\frac{1}{JJ}\cdot\sum_{ii=1}^{JJ} gH(h, ii)^2} \tag{1}$$

Distortion rates, including Total Harmonic Distortion (THD), are likewise aggregated over time, following the same approach as that used for the basic frequency groupings, as shown for example for the THD distortion rate in equation (2). The way of aggregating in time without

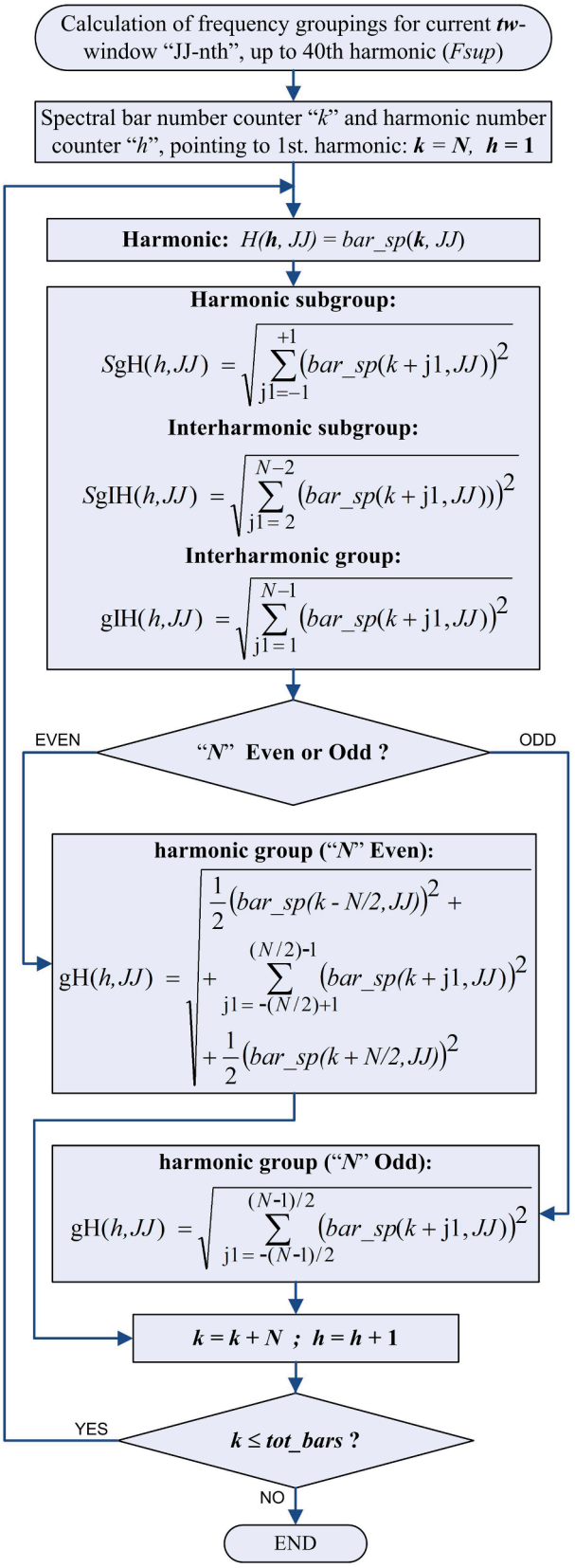

Fig. 5. Flow of grouping calculations up to the 40th harmonic (*Fsup*), for the current *tw* window "JJ-sima".

gaps or resynchronization and without measurement overlaps has been chosen (as indicated in the IEC 61000-4-30 standard for the measurement of harmonics and interharmonics).

$$THD\_aggreg(JJ) = \sqrt{\frac{1}{JJ}\sum_{ii=1}^{JJ} THD(ii)^2} = \sqrt{\frac{1}{JJ}\sum_{ii=1}^{JJ}\left(\sqrt{\sum_{h=2}^{40}\left(\frac{H(h,ii)}{H(1,ii)}\right)^2}\right)^2} \quad (2)$$

3.3. Synchronization of measurements

The proposed measurement system uses rectangular sampling windows, synchronized with the real value of the fundamental harmonic, using as reference signal one of the phase voltages previously filtered in order to extract its fundamental harmonic. Thanks to the use of a high sampling frequency, it is sufficient to vary the number of samples in each analyzed window and thus its duration, depending on the true fundamental period measured. It was therefore not necessary to apply interpolations or other transformations of the analyzed signals, as well as variable sampling rates. The subsequent use of the DFT to analyze the signal, using the current versions of Matlab, does not require obtaining a power-of-two number of samples, as would be required if FFT were used, so interpolation is not necessary for this purpose either.

The technique used to divide the total aggregation time *Tw* into short *tw* windows is based on the detection of zero crossings of the fundamental component of the signal. Further details of this process are given in the flowchart in Fig. 6. It starts with a digital low-pass filtering of the signal used as reference in order to use the cleanest possible part containing the fundamental harmonic. Next, each of the *n* samples of this

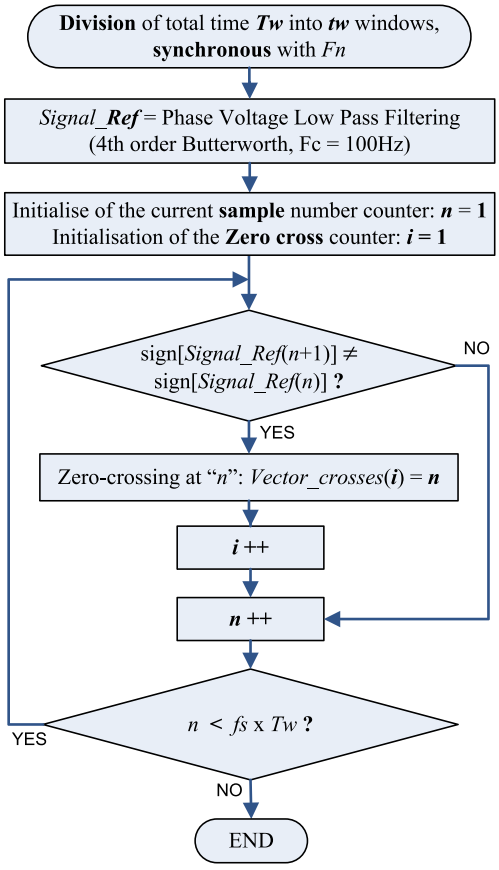

Fig. 6. Flow of the splitting method of the analyzed signal, during the total time aggregation *Tw*, in short *tw* windows.

reference signal is looped through the total "*Fs·Tw*" samples considered, and those whose values differ in sign with respect to the following ones are noted as the samples in which zero crossings occur. Each position of the consecutive samples that change sign is stored in a vector of zero crossings. These positions indicate the beginnings of the periods of the main harmonic, which, in a sinusoidal signal, occur every two zero crossings. The vector of zero crossings obtained will be used to point to the signal samples at the beginning and end instants of each successive basic tw_r window, as indicated in the main flow of Fig. 4 for obtaining the low-resolution DFTs.

The actual duration of each short tw_r analysis window may vary over the total *Tw* acquisition time due to fundamental frequency tolerance and zero-crossing errors (related to noise and interharmonics). But the main difference between each tw_r analysis window and the standard value of about 0.2 s is that the drive output frequency need not be an exact multiple of 5 Hz. In particular, for inverter output frequencies *Fn* between 40 and 60 Hz, the true durations of the short analysis windows tw_r and the consequent frequency resolutions Df_r obtained would range between the values shown in Fig. 7, where the integer number *N* of periods of the fundamental *Fn* contained in each short window tw_r to be as close as possible to 0.2 s is also indicated.

As can be seen in Fig. 7, for frequencies *Fn* multiple of the standard resolution of 5 Hz, the real short window tw_r is just 0.2 s. For the rest of the *Fn* values, the duration of tw_r is approximated to this value of 0.2 s, indicated by the standard 61000-4-7 for network signals.

The actual size of the short window or time resolution tw_r, to fit the integer number of periods of *Fn* closest to the theoretical size of $tw_t = 0.2$ s, varies (hyperbolically) around each frequency *Fn* multiple of the theoretical resolution 5 Hz (see Fig. 7 (a)). Therefore, the actually obtained frequency resolution Df_r also oscillates around these same points, this time linearly (Fig. 7 (b)), being the inverse of the resolution in time tw_r. As can be seen in the same Fig. 7, the largest deviations from the

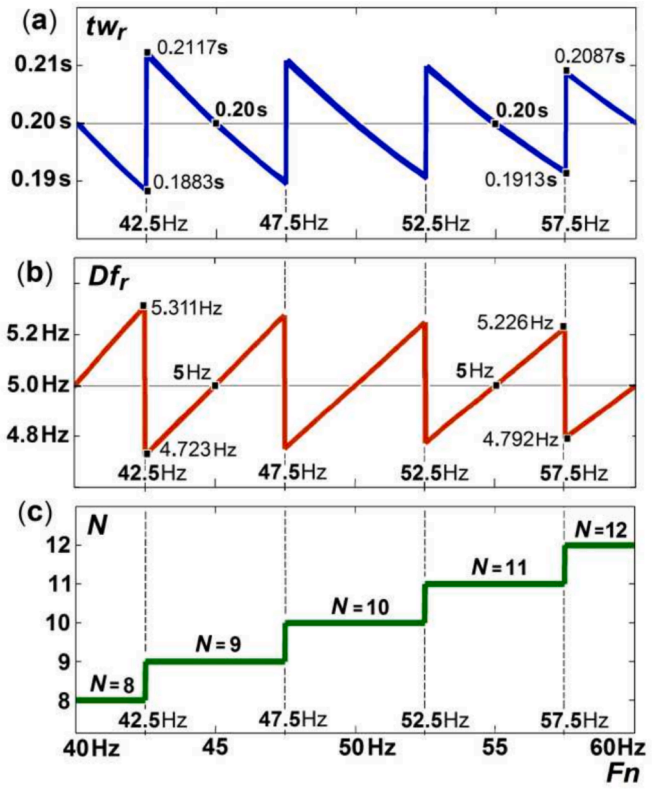

Fig. 7. Actual duration of the analysis windows tw_r (a), actual frequency resolution Df_r (b), and the most approximate number *N* of periods completing the standard short window (c), as a function of the output frequency *Fn*.

standard window value of 0.2 s are obtained for frequencies *Fn* with intermediate values between multiples of 5 Hz. The value of the integer number of *Fn* periods contained in tw_r, *N*, is set for this purpose to the nearest integer part of the quotient between the actually measured *Fn* frequency and the theoretical resolution Df_t (5 Hz): N=round (Fn / Df_t). Thus, the actual value of the analysis window used for each inverter output frequency *Fn* will be:

$$tw_r = N\cdot(1/Fn) = round(Fn/Df_t)\cdot(1/Fn) \quad (3)$$

which will coincide exactly with $1/Df_t$ (i.e. 1/5 Hz = 0.2 s) when *Fn* is a multiple of the ideal resolution Df_t. For example, for frequencies *Fn* between 40 and 60 Hz, *N* will adopt values between 8 and 12 periods of *Fn*, as shown in the same Fig. 7 (c).

As an exact synchronization between analysis window, fundamental harmonic and sampling frequency is not possible, certain margins of error must be allowed for:

- The maximum error allowed by the standards is 0.03 % of the short window analyzed, i.e. 60 us for a short window of $tw_t = 0.2$ s. If the window were larger, it would also admit greater error (for example, for a $tw = 0.4$ s the maximum error would be 120 us), as in fact happens with the outputs of drives whose frequency *Fn* is variable and with it the actual size of the analysis window used.
- The error due to sampling, for a frequency of 80 kS/s, as used in the developed measurement system, is 12.5 us (which improves the error allowed by the standard). Then the sampling error decreases with the sampling frequency. For a given sampling frequency, this error will be smaller in percentage terms the larger the analysis window, since the synchronism error is calculated relative to the actual size of the window (and the larger the analysis window with respect to the sampling error, the smaller the spectral leakage produced).

However, the error arising from synchronism is not solely attributed to signal sampling resolution. The zero crossing point detection method is robust and with low computational burden, but it can be sensitive to noise and harmonic and interharmonic distortions that can deviate the crossing point. It is therefore important to verify that the total error committed does not exceed the margin indicated in the standards. Next, such verification is shown via simulation while in Section 4 a real signal is used for such purpose.

Fig. 8 shows a 230 Vrms phase voltage simulation with frequency varying linearly between 40 and 60 Hz (Chirp-type) over 60 s, to which white noise with 15 dB S/N ratio is added. Shown above are the measured fundamental frequencies after each short window analyzed tw_i (a) and their relative errors for an $Fs = 80$ kS (b) and for an $Fs = 40$ kS (c) with an analysis window as close as possible to 0.2 s in both cases, and with an analysis window as close as possible to 0.4 s in the lower plot (e). The integer number of periods *N* needed to complete the sampling window has been adjusted to the closest possible value to the reference window for each resolution (windows of about 0.2 s if the resolution is 5 Hz, and about 0.4 s for 2.5 Hz), according to the value of the simulated frequency at each instant, as shown in plots (d) and (f).

It can be observed in the graphs of Fig. 8 that the synchronism errors decrease with the sampling frequency *Fs* and with the size of the short analysis window chosen: the highest errors are observed for a frequency $Fs = 40$ kS, with $tw_r \approx 0.2$ s (as shown in graph (c)), which decrease when the sampling frequency is increased to $Fs = 80$ kS (graph (b)), and are further reduced if the analysis window is also increased to 0.4 s (graph (e)). This demonstrates the influence of the size of the analysis window *tw*, and of the output frequency *Fn* and sampling frequency *Fs* on the detected synchronism errors, according to the expression of equation (4):

$$Error(\%) = 100/(Fs\cdot tw_r) = 100\cdot Fn/(Fs\cdot N) \quad (4)$$

since the size of the real window tw_r used for each frequency *Fn* is *N* times the period of *Fn*, i.e. $tw_r = N / Fn$, so the synchronism error also

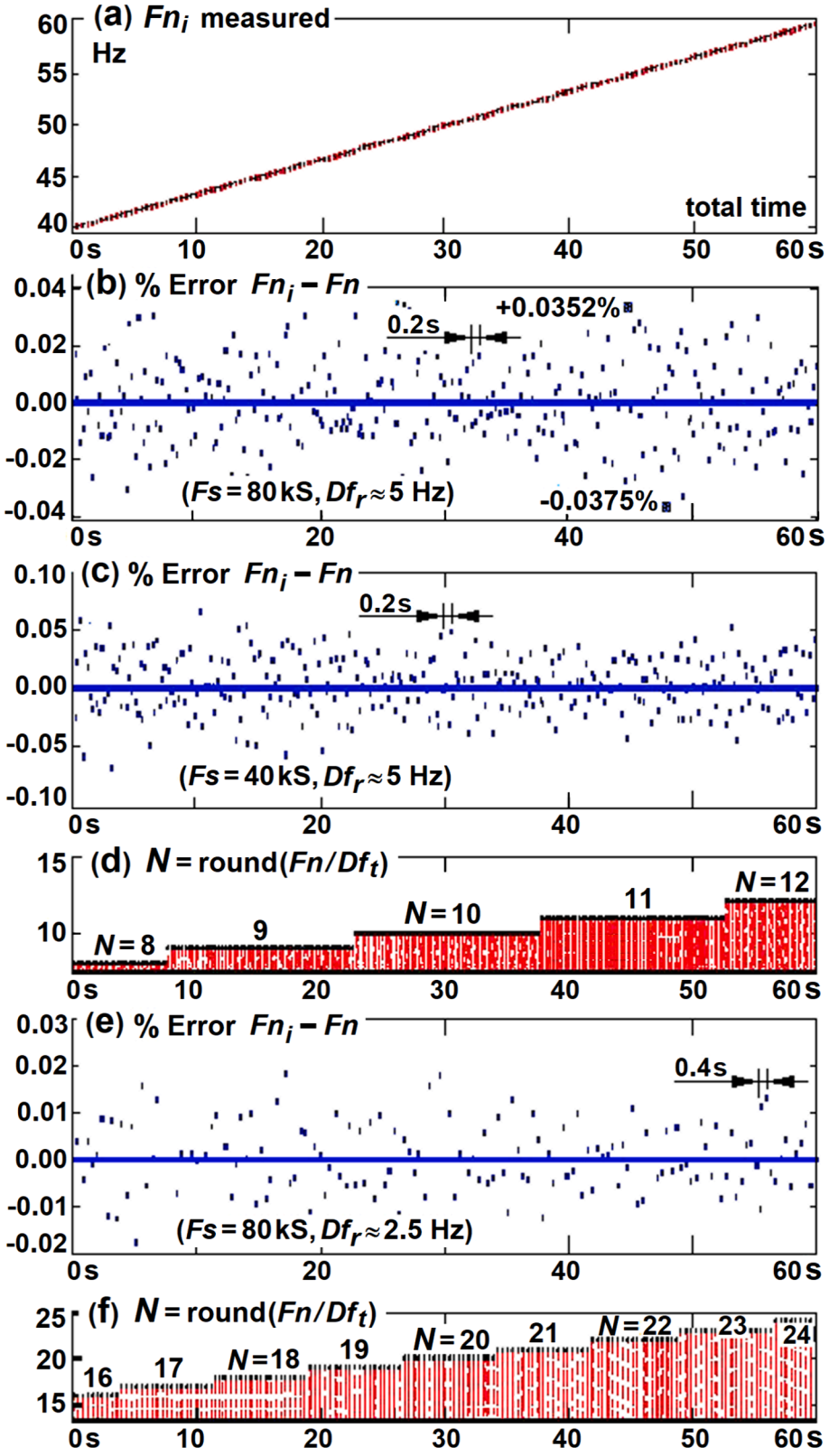

Fig. 8. Simulation of phase voltage with frequency which varies between 40 and 60 Hz over Tw = 60 s.

depends on the particular output frequency of the drive. This expression only considers the sampling error, but in the presence of noise and interharmonics this error increases.

4. Results and discussions

To validate the developed system, this section presents measurement examples focusing on an induction motor whose shaft is attached to a magnetic brake that acts as a mechanical load as shown in Fig. 9.

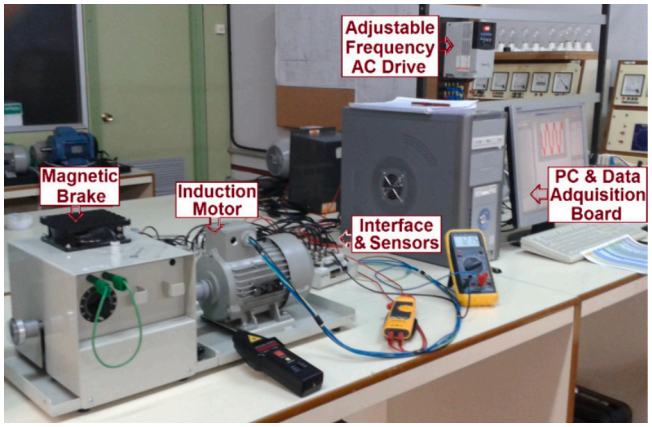

Fig. 9. Test bench.

The ASDs used in the tests of the measurement system are for low power, consisting of an uncontrolled rectifier and a voltage source inverter, so that the greatest harmonic contribution to the load-motor side is due to the inverter located at its output. Specifically, the inverter models used were the AllenBradley PowerFlex 40, with sinusoidal PWM modulation and both scalar and vector control, and the Telemecanique Altivar 66 with closed-loop modulation with constant torque control and also modulation with random carrier frequency for low noise. These models were chosen precisely to have a wider variety of harmonic spectra to analyze, especially in the high frequency range, due to their different control and modulation modes. The rated values of the connected motor were 750 W, 400 V, 1.86 A, 50 Hz, loaded with a magnetic powder brake, operating at both low and high load (slip between 0.3 % and 4 %).

First, an example of verification of the synchronism method used is shown in Fig. 10, with signals from a real test with the Telemecanique Altivar drive, working with closed-loop control (constant torque mode), with fundamental drive output frequency $Fn \approx 55$ Hz constant, exciting an induction motor with mixed eccentricity and nominal load. The total analysis time was $Tw = 60$ s, with a sampling frequency $Fs = 80$ kHz and using the standard resolution of $Df_t = 5$ Hz. Above, in the upper part of the figure we observe the results synchronizing with the stator current I_L, with the current waveform before filtering (a), and the relative errors (c) of the measured fundamental frequencies after each short window analyzed (b). Below are the results synchronizing with the phase voltage V_F, with the voltage waveform before filtering (d) and the relative errors (e) of the measured frequencies using this voltage as reference. As can be seen, taking the phase voltage as a reference yields lower synchronism errors (around a maximum of ± 0.02 %) than with the current (±0.1 %). This is because the voltage, despite its apparent worse waveform (Fig. 10 (d)), has higher amplitude and lower harmonic content near the fundamental than the current. Interharmonics close to the fundamental cause poor detection of zero crossings and are difficult to filter out. Therefore, it is preferable to use the voltage signal as the sync reference, once filtered. This reference signal is used to divide the total analyzed time into short windows, while the pre-filtered signal is the one actually analyzed.

In all the following figures the results are normalized with respect to the fundamental, thus avoiding normalizing between the fundamental subgroup, with possible adjacent bands due to unwanted interharmonics (such as those caused by motor faults like eccentricity or broken rotor bars). This also does not take into account possible sidebands due to amplitude modulation of the fundamental, more likely in network signals measured with conventional methods.

Fig. 11 shows the current spectrum of a PowerFlex drive, with scalar control, $Fn = 50$ Hz and switching frequency 4 kHz, feeding a motor with mixed eccentricity running at full load. The figure shows the lower part of the current spectrum using first a traditional Fourier transform,

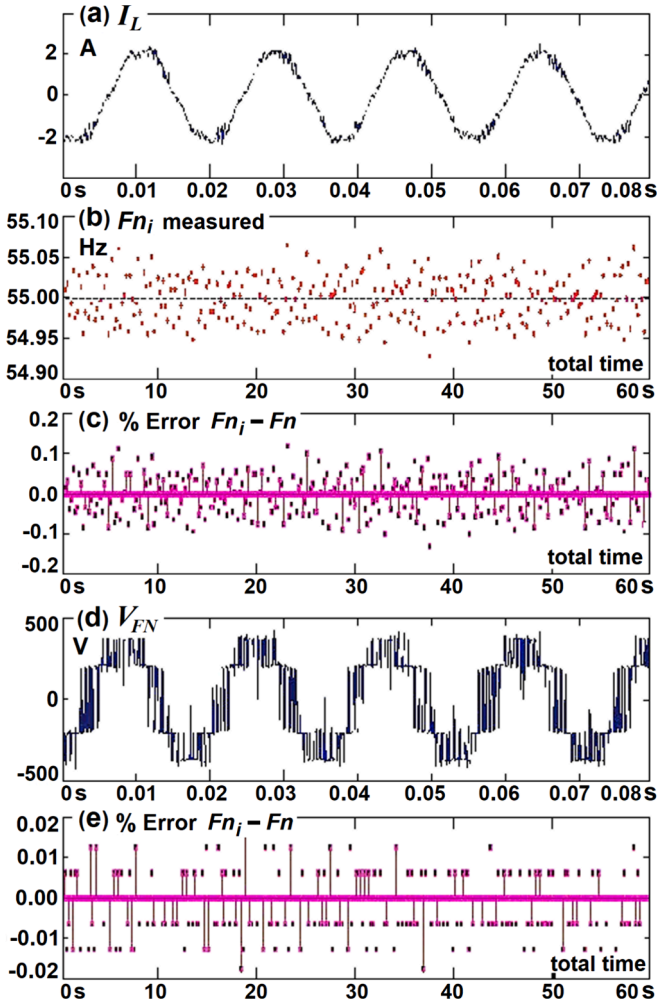

Fig. 10. Synchronization with real test signals with Altivar drive exciting induction motor.

(section (a) of the figure), with large sampling window (10 s) and not synchronized, so high frequency resolution (0.1 Hz) but low time resolution is achieved. This window of 10 s is too large for the pseudo-stationary nature of the drive signals, which, although it shows a high frequency resolution, has a low time resolution and thus does not take into account the lower stationarity of the drive signals. On the other hand, with the method proposed, in sections (b-e) of the figure, short windows of 0.2 s synchronized with the fundamental (giving rise to spectral bars every 5 Hz) aggregated in time (10 s, in 50 windows of 0.2 s) are used, and also aggregated in frequency according to the different harmonic groupings based on the IEC standard. Thus, the figure shows the different possibilities of covering all frequencies of the harmonic spectrum according to the standard: with individual spectral bars separated by about 5 Hz (b), with harmonic and interharmonic subgroups (c), with individual harmonics and interharmonic groups (d), and using 200 Hz groups for high frequencies starting from harmonic 40 (e). In each of these solutions to represent the harmonic spectrum (b-e) the same frequency is never repeated in two different groupings, as recommended by the standards.

In the low frequency region (Fig. 11, graphs a-d) interharmonics due to mixed motor eccentricity can be seen, with an amplitude much larger than the rest. These interharmonics cause the interharmonic subgroups (and also groups) SgIH,0 and SgIH,1 to have a large value, and in smaller proportion the subsequent ones, as seen in (c)-(d) of Fig. 11. In the high frequency region (plot e) the typical side frequency bands at multiples of the switching frequency (around 4 kHz, 8 kHz, etc.) that are common in

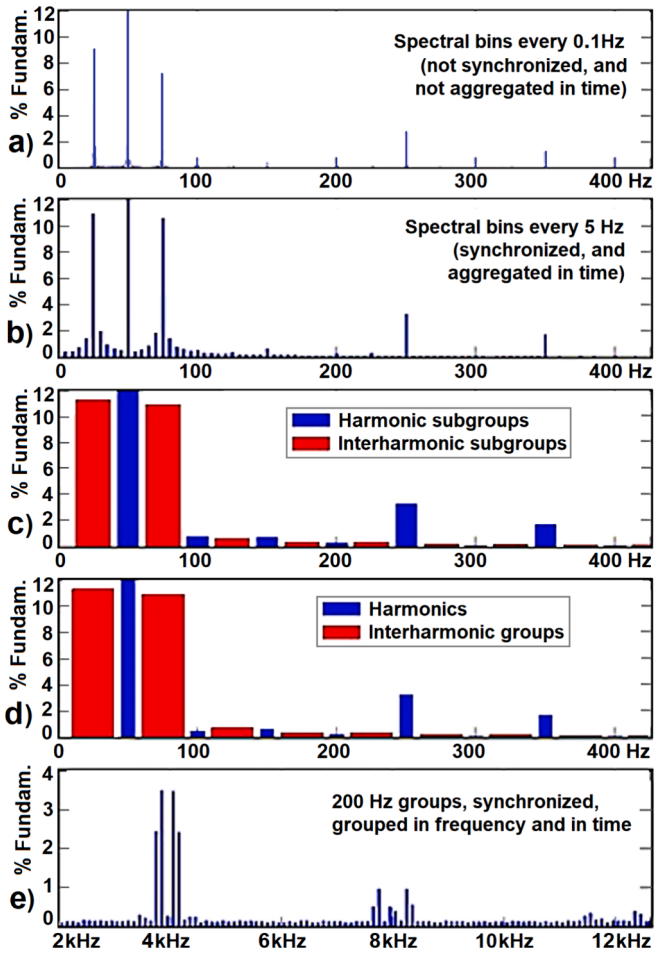

Fig. 11. Different representations of the frequency spectrum of the PowerFlex inverter output current with scalar control and PWM modulation, exciting an induction motor with eccentricity.

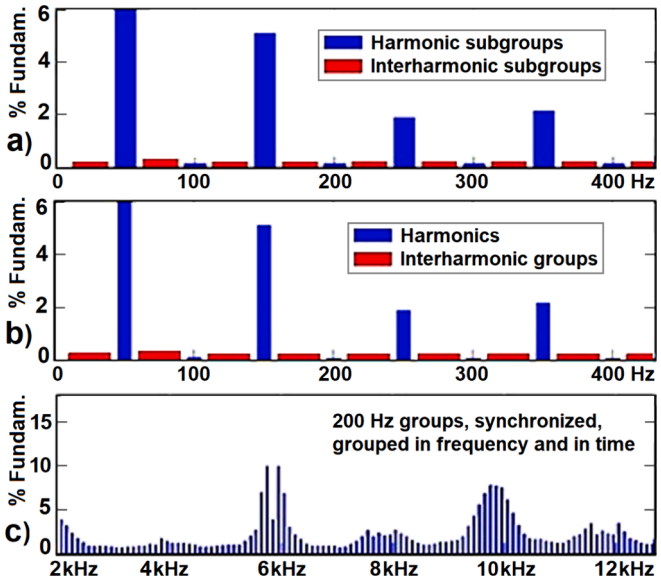

Fig. 12. Frequency spectrum representations of the output voltage of Altivar inverter with closed-loop control and random modulation.

PWM-modulated inverter powering are observed.

Fig. 12 shows the frequency response of the phase-to-neutral voltage output of an Altivar 66 drive, with closed-loop control and random modulation for low acoustic noise, with $Fn = 50$ Hz, exciting an induction motor with eccentricity running at full load. As in Fig. 11, sections (a)-(b) show the low part of the spectrum using the harmonic groupings based on the standard, and section (c) shows the high part of the spectrum, from the 40th harmonic, with 200 Hz groupings. The random modulation modes use a random switching frequency, so that the output harmonics are dispersed, as seen in the high-frequency part (Fig. 12 (c)).

Observing these results, it can be seen that, in general, the harmonic content of the current (Fig. 11) is greater at low frequencies than at high frequencies (contrary to what occurs in the voltage spectrum, Fig. 12). Besides, since the motor filters high frequencies, the current is less distorted than the voltage and the high-frequency part of the current spectrum (Fig. 11(e)) decreases faster with frequency than the voltage (Fig. 12(c)).

Fig. 13 shows the current spectra, for the same drive tested in Fig. 11, as a function of different output frequencies ($Fn = 40$ Hz, 50 Hz and 60 Hz), thanks to the ability of the measurement system developed to analyze different fundamental frequencies, unlike conventional methods that consider fixed frequencies. In all measurements we have always used acquisition windows of 0.2 s (5 Hz spectral bars) synchronized with each fundamental frequency and with aggregations in time of 10 s, thus improving conventional methods that consider insufficient aggregation times of 3 s or excessive aggregation times of 10 min, more appropriate for network signals. In the low frequency part of the spectrum (Fig. 13(a), (b) and (c)), it can be observed that, as the fundamental frequency increases, variations in the odd harmonics occur, typical of the use of overmodulation. Likewise, for all output frequencies, interharmonics around the fundamental are observed, due to the mixed eccentricity of the connected motor. In the high frequency area (Fig. 13(d), (e) and (f)) it can be seen how, as the fundamental frequency increases, the amplitudes and positions of the side bands change around the multiples of the switching frequency, since this is a PWM modulated drive.

Concerning distortion rates, Fig. 14 shows the total harmonic and interharmonic rates of low frequency TH&IHDg$_{LF}$ (up to and including the 40th harmonic), high frequency TH&IHD$_{HF}$ (from the 40th harmonic up to 20 kHz) and high and low frequency TH&IHDg$_{LF\&HF}$, obtained with the Allen-Bradley drive connected to an induction motor with nominal load, when changing the output fundamental frequency. A similar distribution is seen between the low and high frequency total current rates (a). The low-frequency TH&IHD$_{LF}$ current rate increases with the drive output frequency, as seen in Fig. 14(a), mainly due to the increase of harmonic components due to overmodulation and motor eccentricity (as also seen in Fig. 13(a)-(c)). In contrast, the high-frequency harmonic content measured by the voltage TH&IHD$_{HF}$ rate (b) is much higher than the corresponding low-frequency TH&IHD$_{LF}$, so that the total TH&IHD$_{LF\&HF}$ voltage rate is mainly composed of the TH&IHD$_{HF}$ rate. Furthermore, it is evident that the voltage rate decreases as the output fundamental frequency increases, reaching a stable level beyond the nominal frequency.

5. Conclusions

Adjustable Speed Drive outputs must adjust their fundamental frequencies to control motor speed, producing a varied and significant harmonic and interharmonic content across a broad frequency range that may exceed the limits specified in power quality measurement standards. Thus, the need arises for a specialized measurement system tailored to accurately capture and analyze such signal characteristics. To solve this problem, this work presents a novel measurement and spectral analysis procedure for the experimental characterization of frequency inverters feeding induction motors, according to the harmonic content

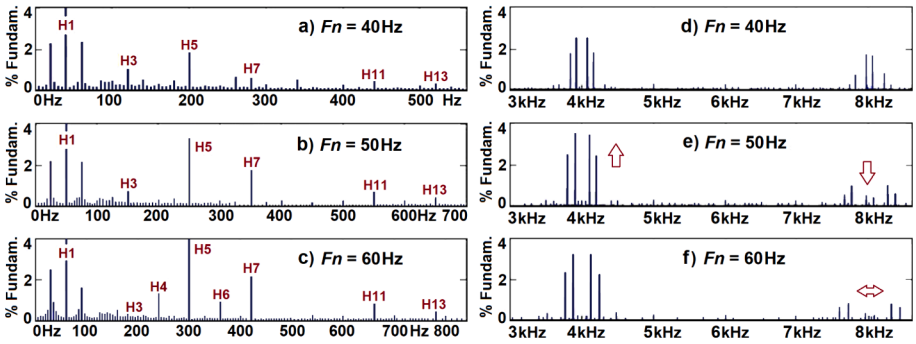

Fig. 13. Frequency response of the Allen Bradley drive output current, with PWM modulation and feeding induction motor, for various output frequencies.

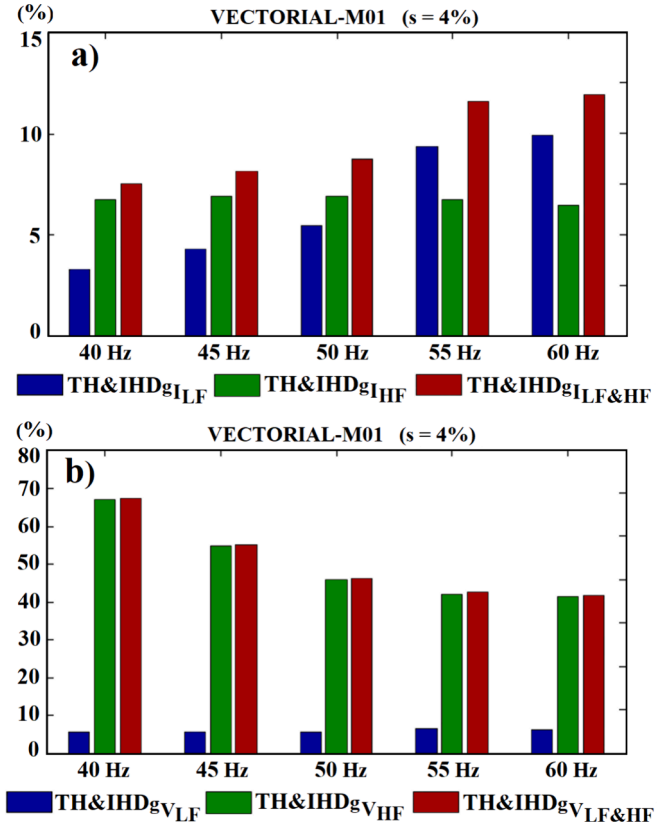

Fig. 14. Relationships between harmonic and interharmonic rates of low frequency TH&IHDg$_{LF}$, high frequency TH&IHDg$_{HF}$ and total high and low frequency TH&IHDg$_{LF\&HF}$, when changing the fundamental output frequency, for current (a), and voltage (b).

of their outputs, and thus be able to prevent possible undesired effects on the motors.

The system developed in this paper has been based on IEC standard techniques adapted to the characteristics of the output signals of the inverters, being able to measure harmonics and interharmonics, both at low and high frequencies, and to present synchronization capacity with variable fundamental frequencies and different from that of the network, also allowing to adapt the aggregation times and frequency groupings and distortion rates to the characteristics of the inverter signals. For this purpose, the DFT transform has been used on short analysis windows, synchronized with the fundamental and sampling periods in order to reduce the generation of spectral leakage, and grouping has been performed both in time and frequency to minimize the effects of leakage.

In addition to the above it can be concluded:

- Using the phase voltage as a reference signal, instead of the stator current, has yielded lower synchronism errors. This is attributed to the presence of interharmonics near the current fundamental, resulting from motor faults. These factors hinder the accurate detection of zero crossings, further supporting the preference for phase voltage as a more reliable reference signal.
- The designed harmonic measurement system has presented synchronism errors below the limits set in the standards. For this purpose, the analysis window has been synchronized with all the different fundamental frequencies used by the drives, choosing the phase voltage as the synchronism reference, and selecting a sampling frequency high enough to sufficiently reduce the synchronism errors, without the need for interpolation. The use of DFTs, rather than FFTs, has also avoided the need for interpolation and its associated errors.
- Experimental results have been obtained with the developed measurement system. From these results, the presence of current interharmonics, mainly due to the connected motor, and a predominance of harmonics as opposed to voltage interharmonics, stand out in the low frequency zone. At high frequencies, harmonics and interharmonics are measured together, with much higher voltage distortion rates than current distortion rates, due to the type of converter tested and the filtering effect of the motor on the current.
- The increase of the aggregation time to improve the accuracy of the measurements, as well as the calculation of the new distortion rates over a wider frequency range, and the synchronization procedure with variable fundamental frequencies, imply a longer processing time for the data analysis, but the hardware required by the developed system is identical to the one used if the original standards were applied without adaptation to the measurement of drive signals.

The developed system thus improves the accuracy of the harmonic estimation process defined in the IEC standards, by selecting the appropriate aggregation times, frequency groupings and distortion rates to be able to evaluate the harmonic distortion correctly at the output of equipment with a strong harmonic and interharmonic content, such as frequency inverters feeding induction motors.

In summary, the developed system has enabled us to gain insights into the harmonic behavior of commercial drives under real operating conditions, providing invaluable information that supplements the capabilities of a standard commercial meter when it comes to analyzing such signal characteristics. Further research should be carried out on existing methods to improve the accuracy of interharmonic and high frequency measurements, and the frequency-time resolutions and aggregation times that minimize the effects of leakage optimally in the case of higher power drives. Similarly, tests should be performed with more drives, with more forms of control and modulation, in order to confirm the validity of this measurement system and further apply it to the harmonic characterization of ASDs.

CRediT authorship contribution statement

Angel Arranz-Gimon: Writing – original draft, Software, Methodology, Data curation, Conceptualization. **Angel Zorita-Lamadrid:** Writing – original draft, Supervision, Data curation, Validation. **Daniel Morinigo-Sotelo:** Supervision, Methodology, Conceptualization. **Vanesa Fernandez-Cavero:** Writing – review & editing, Data curation. **Oscar Duque-Perez:** Writing – review & editing, Validation, Supervision.

Declaration of competing interest

The authors declare that they have no known competing financial interests or personal relationships that could have appeared to influence the work reported in this paper.

Data availability

Data will be made available on request.

References

[1] Soltani H, Davari P, Zare F, Blaabjerg F. Effects of modulation techniques on the input current interharmonics of adjustable speed drives. IEEE Trans Ind Electron 2018;65:167–78. https://doi.org/10.1109/TIE.2017.2721884.

[2] Poorfakhraei A, Narimani M, Emadi A. A review of modulation and control techniques for multilevel inverters in traction applications. IEEE Access 2021;9:24187–204. https://doi.org/10.1109/ACCESS.2021.3056612.

[3] Leon JI, Kouro S, Franquelo LG, Rodriguez J, Wu B. The essential role and the continuous evolution of modulation techniques for voltage-source inverters in the past, present, and future power electronics. IEEE Trans Ind Electron 2016;63:2688–701. https://doi.org/10.1109/TIE.2016.2519321.

[4] Merizalde Y, Hernández-Callejo L, Duque-Perez O. State of the art and trends in the monitoring, detection and diagnosis of failures in electric induction motors. Energies 2017;10:1056. https://doi.org/10.3390/en10071056.

[5] Allal A, Khechekhouche A. Diagnosis of induction motor faults using the motor current normalized residual harmonic analysis method. Int J Electr Power Energy Syst 2022;141:108219. https://doi.org/10.1016/j.ijepes.2022.108219.

[6] Saucedo-Dorantes JJ, Jaen-Cuellar AY, Delgado-Prieto M, Romero-Troncoso R de J, Osornio-Rios RA. Condition monitoring strategy based on an optimized selection of high-dimensional set of hybrid features to diagnose and detect multiple and combined faults in an induction motor. Meas. J. Int. Meas. Confed. 2021;178:109404. https://doi.org/10.1016/j.measurement.2021.109404.

[7] Elvira-Ortiz DA, Morinigo-Sotelo D, Duque-Perez O, Osornio-Rios RA, Romero-Troncoso RJ. Study of the harmonic and interharmonic content in electrical signals from photovoltaic generation and their relationship with environmental factors. J Renew Sustain Energy 2019;11:43502. https://doi.org/10.1063/1.5094038.

[8] Al Hadi FM, Aly HH, Little T. Harmonic forecasting of wind and solar hybrid model driven by DFIG and PMSG using ANN and ANFIS. IEEE Access 2023;11:55413–24. https://doi.org/10.1109/ACCESS.2023.3253047.

[9] J. Hernandez, A.A. Romero, S. Muller, J. Meyer, Harmonic Distortion in Low Voltage Residential Grids Caused by LED Lamps, Proc. Int. Conf. Harmon. Qual. Power, ICHQP. 2022-May (2022) 25-30. doi:10.1109/ICHQP53011.2022.9808589.

[10] Srivastava A, Manas M, Dubey RK. Electric vehicle integration's impacts on power quality in distribution network and associated mitigation measures: a review. J Eng Appl Sci 2023;70:1–29. https://doi.org/10.1186/s44147-023-00193-w.

[11] H. Soltani, P. Davari, D. Kumar, F. Zare, F. Blaabjerg, Effects of DC-link filter on harmonic and interharmonic generation in three-phase adjustable speed drive systems, 2017 IEEE Energy Convers. Congr. Expo. ECCE 2017. 2017-Janua (2017) 675-681. doi: 10.1109/ECCE.2017.8095849.

[12] Di. Yang, Z. Zhou, Y. Liu, J. Jiang, Modeling of Dual-PWM Adjustable Speed Drives for Characterizing Input Interharmonics Due to Torque Oscillations, IEEE J. Emerg. Sel. Top. Power Electron. 9 (2021) 1565-1577. doi: 10.1109/JESTPE.2020.2983876.

[13] Moradi A, Farajizadeh F, Zare F, Kumar D, Rathnayake H, Sharma R, et al. Detailed estimation of grid-side current and its oscillations caused by adjustable speed drive systems. IEEE Trans Ind Electron 2022;70:8777–87. https://doi.org/10.1109/TIE.2022.3206695.

[14] S.K. Ronnberg, A.G. De Castro, M.H.J. Bollen, A. Moreno-Munoz, E. Romero-Cadaval, Supraharmonics from power electronics converters, Proc. - 2015 9th Int. Conf. Compat. Power Electron. CPE 2015. (2015) 539-544. doi: 10.1109/CPE.2015.7231133.

[15] Alfalahi STY, Alkahtani AA, Al-Shetwi AQ, Al-Ogaili AS, Abbood AA, Bin Mansor M, et al. Supraharmonics in power grid: Identification, standards, and measurement techniques. IEEE Access 2021;9:103677–90. https://doi.org/10.1109/ACCESS.2021.3099013.

[16] Michalec Ł, Kostyła P, Leonowicz Z. Supraharmonic pollution emitted by nonlinear loads in power networks-ongoing worldwide research and upcoming challenges. Energies 2023;16. https://doi.org/10.3390/en16010273.

[17] International Electrotechnical Commission (IEC), ed., IEC Standard 61000-4-7: General Guide on Harmonics and Interharmonics Measurements, for Power Supply Systems and Equipment Connected Thereto, IEC, Geneva, Switzerland, 2004 + A1: 2010.

[18] International Electrotechnical Commission (IEC), ed., IEC Standard 61000-4-30: Testing and Measurement Techniques-Power Quality Measurement Methods, IEC, Geneva, Switzerland, 2015.

[19] Tarasiuk T. Comparative study of various methods of DFT calculation in the wake of IEC standard 61000-4-7. IEEE Trans Instrum Meas 2009;58:3666–77. https://doi.org/10.1109/TIM.2009.2019308.

[20] Hui J, Yang H, Xu W, Liu Y. A method to improve the interharmonic grouping scheme adopted by IEC standard 61000-4-7. IEEE Trans Power Deliv 2012;27:971–9. https://doi.org/10.1109/TPWRD.2012.2183394.

[21] Brnobić D, Vlahinić S, Stojković N. The effect of IEC grouping algorithms on frequency domain noise. Meas J Int Meas Confed 2010;43:426–33. https://doi.org/10.1016/j.measurement.2009.12.013.

[22] Lodetti S, Bruna J, Melero JJ, Sanz JF. Wavelet packet decomposition for IEC compliant assessment of harmonics under stationary and fluctuating conditions. Energies 2019;12. https://doi.org/10.3390/en12224389.

[23] Arranz-Gimon A, Zorita-Lamadrid A, Morinigo-Sotelo D, Duque-Perez O. Analysis of the use of the Hanning Window for the measurement of interharmonic distortion caused by close tones in IEC standard framework. Electr Power Syst Res 2022;206:107833. https://doi.org/10.1016/j.epsr.2022.107833.

[24] Artale G, Caravello G, Cataliotti A, Cosentino V, Ditta V, Di Cara D, Panzavecchia N, Tinè G, Dipaola N, Sambataro MG. Measurement issues on harmonic analysis according to the IEC 61000-4-7. 25th IMEKO TC-4 Int. Symp. Meas. Electr. Quant. IMEKO TC-4 2022 23rd Int. Work. ADC DAC Model. Testing, IWADC 2022 2022:187–92. https://doi.org/10.21014/tc4-2022.35.

[25] Ritzmann D, Lodetti S, De La Veg D, Khokhlov V, Gallarreta A, Wright P, et al. Comparison of measurement methods for 2–150-kHz conducted emissions in power networks. IEEE Trans Instrum Meas 2021;70:1–10. https://doi.org/10.1109/TIM.2020.3039302.

[26] Lodetti S, Bruna J, Melero JJ, Khokhlov V, Meyer J. A robust wavelet-based hybrid method for the simultaneous measurement of harmonic and supraharmonic distortion. IEEE Trans Instrum Meas 2020;69:6704–12. https://doi.org/10.1109/TIM.2020.2981987.

[27] Grasel B, Reis MJCS, Baptista J, Tragner M. Comparison of Supraharmonic emission measurement methods using real signals of a V2G charging station and a PV power plant. SEST 2022 - 5th Int Conf Smart Energy Syst Technol 2022:2–7. https://doi.org/10.1109/SEST53650.2022.9898483.

[28] A. Gallarreta, I. Fernandez, D. Ritzmann, S. Lodetti, V. Khokhlov, P. Wright, J. Meyer, D. De La Vega, Adaptation of the IEC 61000-4-7 Measurement Method to CISPR Band A (9-150 kHz), 2022 12th IEEE Int. Work. Appl. Meas. Power Syst. AMPS 2022 - Proc. (2022). doi: 10.1109/AMPS55790.2022.9978818.

[29] Chen CI, Chen YC. Comparative study of harmonic and interharmonic estimation methods for stationary and time-varying signals. IEEE Trans Ind Electron 2014;61:397–404. https://doi.org/10.1109/TIE.2013.2242419.

[30] Bollen MHJ, Gu IYH. Signal processing of power quality disturbances. Wiley-IEEE Press 2006. https://doi.org/10.1002/0471931314.

[31] Liu Y, Wang X, Liu Y, Cui S. Resolution-enhanced harmonic and interharmonic measurement for power quality analysis in cyber-physical energy system. Sensors (Switzerland) 2016;16:946. https://doi.org/10.3390/s16070946.

[32] Duc ML, Bilik P, Martinek R. Harmonics signal feature extraction techniques: A review. Mathematics 2023;11. https://doi.org/10.3390/math11081877.

[33] Jain SK, Singh SN. Harmonics estimation in emerging power system: Key issues and challenges. Electr Power Syst Res 2011;81:1754–66. https://doi.org/10.1016/j.epsr.2011.05.004.

[34] Y. Shin, A.C. Parsons, E.J. Powers, W.M. Grady, Time-frequency analysis of power system disturbance signals for power quality, 1999 IEEE Power Eng. Soc. Summer Meet. PES 1999 - Conf. Proc. 1 (1999) 402-407. doi: 10.1109/PESS.1999.784382.

[35] P.M. Oliveira, V. Barroso, Uncertainty in the time-frequency plane, in Proc. IEEE 10th Workshop Statist. Signal Array Process (2000) 607–611. doi:10.1109/SSAP.2000.870197.

[36] Gu Y, Bollen MHJ. Time-frequency and time-scale domain analysis of voltage disturbances. IEEE Trans Power Deliv 2000;15:1279–84. https://doi.org/10.1109/61.891515.

[37] Oliveira WR, Filho ALF, Cormane J. A contribution for the measuring process of harmonics and interharmonics in electrical power systems with photovoltaic sources. Int J Electr Power Energy Syst 2019;104:481–8. https://doi.org/10.1016/j.ijepes.2018.07.018.

[38] Union of the Electricity Industry Eurelectric, ed., Application guide to the European Standard EN 50160 on "voltage characteristics of electricity supplied by public distribution systems". Electricity Product Characteristics and Electromagnetic Compatibility, Ref, 23002Ren9530, 1995.

[39] Tarasiuk T. A few remarks about assessment methods of electric power quality on ships - Present state and further development. Measurement 2009;42:1153–63. https://doi.org/10.1016/j.measurement.2008.02.003.

[40] Barros J, Diego RI. On the use of the Hanning window for harmonic analysis in the standard framework. IEEE Trans Power Deliv 2006;21:538–9. https://doi.org/10.1109/TPWRD.2005.852339.

[41] J. Barros, R.I. Diego, Effects of windowing on the measurement of harmonics and interharmonics in the IEC standard framework, in: Conf. Rec. - IEEE Instrum. Meas. Technol. Conf., 2006: pp. 2294-2299. doi: 10.1109/IMTC.2006.328581.

[42] Salor Ö. Spectral correction-based method for interharmonics analysis of power signals with fundamental frequency deviation. Electr Power Syst Res 2009;79: 1025–31. https://doi.org/10.1016/j.epsr.2008.12.016.
[43] Aiello M, Cataliotti A, Cosentino V, Nuccio S. Synchronization techniques for power quality instruments. IEEE Trans Instrum Meas 2007;56:1511–9. https://doi.org/10.1109/TIM.2007.903585.
[44] Arranz-Gimon A, Zorita-Lamadrid A, Morinigo-Sotelo D, Duque-Perez O. A Study of the effects of time aggregation and overlapping within the framework of IEC standards for the measurement of harmonics and interharmonics. Appl Sci 2019;9: 4549. https://doi.org/10.3390/app9214549.
[45] A. Arranz-Gimon, A. Zorita-Lamadrid, D. Morinigo-Sotelo, O. Duque-Perez, A Review of Total Harmonic Distortion Factors for the Measurement of Harmonic and Interharmonic Pollution in Modern Power Systems, Energies 2021, Vol. 14, Page 6467. 14 (2021) 6467. doi: 10.3390/EN14206467.